Aerospace Science and Technology 112 (2021) 106557

Contents lists available at ScienceDirect

Aerospace Science and Technology

www.elsevier.com/locate/aescte

Design, aerodynamic analysis and test flight of a bat-inspired tailless flapping wing unmanned aerial vehicle

Dawei Bie, Daochun Li *, Jinwu Xiang, Huadong Li, Zi Kan, Yi Sun

School of Aeronautic Science and Engineering, Beihang University, Beijing, China

ARTICLE INFO

Article history:
Received 5 February 2020
Received in revised form 13 October 2020
Accepted 2 February 2021
Available online 25 February 2021
Communicated by Huihe Qiu

Keywords:
Bat-inspired
Flapping wing
UAV
Aerodynamic analysis
Test flight

ABSTRACT

This paper provided a design of bat-inspired tailless flapping wing unmanned aerial vehicle (UAV) based on the biological data of the large flying fox. The wing span of the UAV is 1.68 m and the total mass is 289 g. Aerodynamic characteristics at design cruise speed were analyzed based on the computational fluid dynamics (CFD) method. Selected variables within the analysis are angle of attack and flapping frequency. Prototype of the UAV has been manufactured follows the design parameters. The flapping mechanism employed a 2-DOFs revolute-spherical-spherical-revolute (RSSR) system to reflect the flapping attitude of bats. An outdoor test flight was then processed with the manufactured prototype. Onboard flight data recorder (FDR) was equipped to conserve the flight data such as flight speed, pitching angle and the three-dimensional position of the flight. It is shown by the data obtained from the FDR that the bat-inspired UAV is able to achieve the stable cruise with circular route at flight speed 6.8 m/s with the average angle of attack 4.1 degrees and flapping frequency 3.7 Hz. Test flight shows that the UAV is able to provide a 5 minutes free outdoor cruise with the equipped Li-Po battery. Research proves that the tailless configuration flapping wing UAV is able to sustain a stable flight, which provides a new design possibility for future researches.

1. Introduction

Flapping wing creatures including birds, bats and flying insects have shown superior flight performance because of the high aerodynamic efficiency at low Reynolds number. Substantial research works have been made on the developing of bio-inspired flapping wing unmanned aerial vehicles (UAV) in recent years. In terms of insect inspired area, the optimization of aerodynamic performance is a research focus. Unsteady aerodynamic of an insect wing is processed by Chen et al. [1] with 3D computational fluid dynamics (CFD) simulation to discover the relationship between the aerodynamic lift and wing flexibility. Bayiz et al. [2] created a trajectory optimization system based on the method of experimental learning and particle image velocimetry (PIV) technic. To gain further insight of the flow field and mechanics of the insect flapping wing, an insect-like flapping wing mechanisms with double spherical Scotch yoke was developed by Żbikowski et al. [3,4] to mimic the insect flapping wing motion. Meanwhile, many studies in the field of insect bionics are also addressed to achieve flexible maneuvers similar to real insects. Phan et al. [5] learned the attitude of a beetle through high-speed camera, and then designed an insect-like flapping wing micro aerial vehicle (MAV) to mimic the takeoff attitude. Karasek et al. [6] proposed a tailless MAV to mimic the attitude of fruit fly. The MAV equipped with four wings and employed the asymmetric control scheme to achieve the high maneuverability to imitate the rapid escape maneuvers of flies.

Compared with the insects which guarantee the high maneuverability through complex motions of wings, birds wing are mainly responsible for generating lift and thrust [7]. Many researchers analyzed the influence factors to the aerodynamic property. The performance influenced by wing shape, aspect ratio, angle of attack [8] were analyzed by Gong et al. Xue et al. [9] put forward a flexible multi-body dynamics simulation to analysis the effect of body vibration in aerodynamic lift and thrust. A free flight test was processed and the flight data shows agreement with the computational results. Mazaheri and Ebrahimi [10] processed a wind tunnel test to discover the relationship of the lift and thrust with respect to angle of attacks and flapping frequencies in four different flight speeds. Development in simulation and experiment technic resulted in some successful design concepts. Yang [11] carried out a fluid-structure interaction analysis and designed a bird-like flapping wing MAV which is able to achieve a

* Corresponding author.
E-mail address: lidc@buaa.edu.cn (D. Li).

https://doi.org/10.1016/j.ast.2021.106557
1270-9638/

fully autonomous flight. Tsai and Fu [12] obtained the average lift of a planar membrane wing through 3D aerodynamic calculation firstly, and then made an ultra-light, small size birdlike flapping micro UAV with gross weight less than the average lift.

Different with birds, bats are born with the characteristic of tailless. Tailless configuration in fixed wing aircraft has a series of benefits such as low structural mass, good aerodynamic characteristics [13]. The benefits may also exist when it comes to a flapping wing aircrafts which need to be confirmed by further research. Bats with the inborn tailless feature become an excellent object for imitation of the configuration. Bats have membrane wing between the fore and hind limbs. The sternum and pectoral muscles are well developed which provide bats the ability to fly [14]. Compared with birds, bats are capable of diverse flight performance and able to achieve more complex maneuvers [15–17]. Research difficulties of the bat-inspired UAV including the complex wing motion and unsteady aerodynamics of the large flexibility membrane wing [15,18,19]. Numbers of works have been published in terms of the flapping motion and kinematics of bats [20,21]. The modulation of wing shape under different flight circumstances is discovered and analyzed through wind tunnel test which provided the foundation for the design of bat-inspired UAVs. Ruskin et al. [22] made a comparison of flight kinematics of 27 bats in six pteropodid species. The research provided the relationship of parameters including lift coefficient, wing flapping period and angle of attack with respect to body mass. Power input and aerodynamic force analysis during the flapping period was proceeded with the simplified flapping robotic bat wing designed by Behlman et al. [15] The robotic wing consists of 2-DOFs (vertical and horizontal) scapula and 1-DOF (flexion/extension) elbow and wrist. The energy input and aerodynamic force output during a specific flying case are able to measure directly based on the model. Ramezani et al. [19] designed a bat-inspired UAV named Bat Bot (B2). The B2 has a wing span 0.47 m and the total mass is 93 g. The wing mechanism is simplified into 5-DOFs and is able to achieve symmetric and asymmetric motion, which gives the UAV the ability to process more flexible maneuver during flight. Fabricated prototype is able to achieve indoor flight cases including straight flight, diving and bank turn.

In terms of the design of bat-inspired UAVs, successful works still have problems including low payload capacity and low wind resistance ability, which makes the UAVs only able to provide flight in specific indoor environment. This paper provided the design and test flight of a bat-inspired UAV based on the biological data of the large flying fox. Aerodynamic characteristics at design cruise speed were analyzed based on the CFD simulation. An outdoor test flight was processed with the manufactured prototype. Comparisons between flight data and CFD result were then provided.

2. Geometry and kinematics

2.1. Bionic similarity

The design concept of the bat-inspired UAV in this paper is proposed based on bionics similarity. Tailless configuration is employed thus the frame of the UAV only consists of wing and fuselage. The shape of the wing is selected based on the biological data of the flying fox, *Pteropus* [23]. As shown in Fig. 1, the wing span is selected to be 1.68 m; the area of the wing surface is 0.41 m^2. Detailed geometry data is provided in Table 1. The maximum wingbeat amplitude of the species is around 90 degrees.

Flexible wing with membrane skin is employed to reflect the passive chordwise deformation. The skeleton frame is manufactured using carbon fiber rod structure. The skin of the wing is covered by Polyester fiber material.

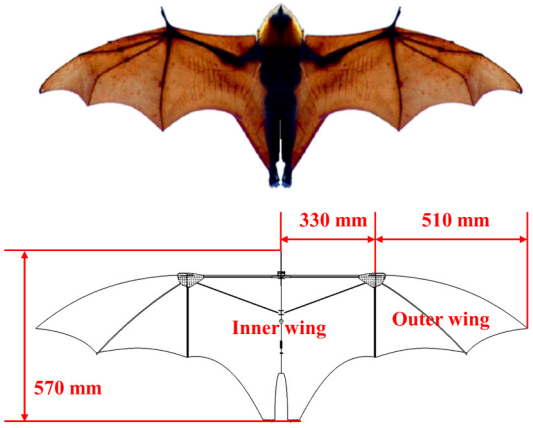

Fig. 1. Bat-inspired UAV frame geometry.

Table 1
Geometry data.

Parameters	Data
Fuselage length	0.57 m
Inner wing semi-span	0.33 m
Outer wing semi-span	0.51 m
Aspect ratio	7

Table 2
Geometry data of the bars in the four bar linkage mechanism.

Bars	Length
Frame link	10 mm
Input link	330 mm
Output link	342 mm
Coupler link	24 mm

2.2. Flapping motion

Bats need to perform flapping with large amplitude during flying [23]. There will be a large flapping angle difference between the outer and inner wing section. In order to reflect the feature, the wing surface of the UAV is separated into inner and outer portions as shown in Fig. 1. A spanwise 2-DOFs flapping motion is designed based on the four bar linkage mechanism as explained in Fig. 2. The consisting components of the four bar mechanism including the frame link, input link, coupler link and output link are all marked in the figure. The dashed line in Fig. 2 represents the initial position and solid line represents the position after the downstroke motion. The wing is flapping with respect to the flapping shaft as an input link while the assist bar is connected to the root of the outer wing which is able to execute a passive rotation with respect to the assist shaft. As shown in Fig. 2, the outer wing is able to perform a different flapping angle with respect to the inner wing during downstroke with the mechanism, which is a separated DOF. The inner wing is able to flap from 30 to −30 degrees while the outer wing flap ranges from 30 to −60 degrees. Detailed lengths of the designed links are provided in Table 2.

The flapping motion of the wing consists of upstroke and downstroke. Each state takes half of a period. For the bat-inspired UAV design in this paper, the inner wing and outer wing shared a same period but have two different flapping amplitudes. The inner wing rotates around the wing root. The flapping angel varies from 30 to −30 degrees. The flapping angle is modeled as follows:

$$\theta_{inner} = 0.5236 \cdot \cos(2\pi f \cdot t) \tag{1}$$

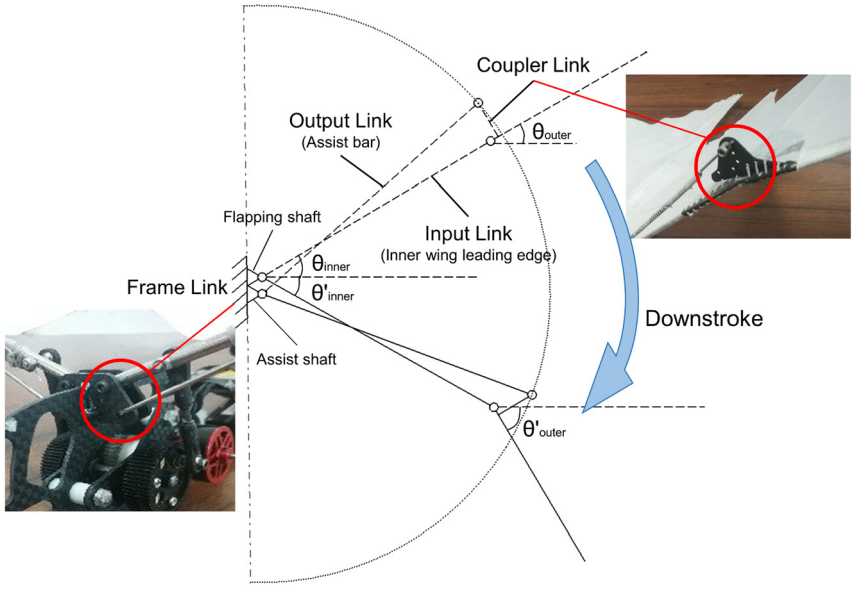

Fig. 2. 2-DOFs flapping motion.

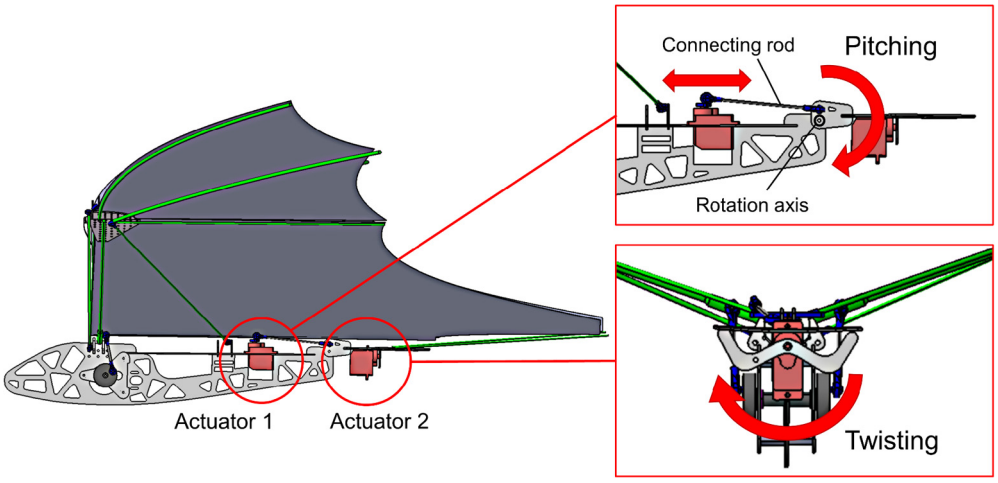

Fig. 3. Control surface arrangement.

The outer wing flaps from 30 to −60 degrees. The flapping motion can also be expressed as a trigonometric formula with the cross line of inner and outer wing as the pivot:

$$\theta_{outer} = 0.7854 \cdot \cos(2\pi f \cdot t) - 0.2618 \tag{2}$$

2.3. Control surface arrangement

The maneuver of the bat-inspired UAV is achieved based on control surfaces arranged on the wing, as same as the flying wing aircrafts [13]. The control mechanism of the bat-inspired UAV employs two actuators as shown in Fig. 3. Actuator 1 is responsible for pitching control. The actuator is able to drive a pitch motion of the control surface with respect to the specific rotation axis through pull or push the connecting rod. Actuator 2 is responsible for twisting the control surface to achieve a roll and yaw mixed control. It is able to observe from the figure that the control surface of the bat-inspired UAV designed in this paper shares the same skin with the wing which resulted in a tailless configuration.

2.4. Initial parameter estimation

The total mass of the bat-inspired UAV is described as follows,

Table 3
Mass specification.

Components		Mass (g)
Motor system	Electric motor	43
	Speed controller	17
Flight control system	Flight controller	25
	Actuators	16
Power system	Battery	40
Data communication	Payload	5

$$M_T = M_c + M_r + M_t + M_e + M_s \tag{3}$$

where M_c is the mass of flight controller system, M_r is the mass of data communicating system, M_t is the motor system mass, M_e is power system mass and M_s is the structure mass, respectively. Detailed mass of the onboard equipment is provided in Table 3. The structural mass is assumed to be $0.5M_T$, thus the total mass is estimated to be 292 g.

Based on the mass property, the flapping frequency can be estimated with the empirical equation obtained from the biological data as follows [7],

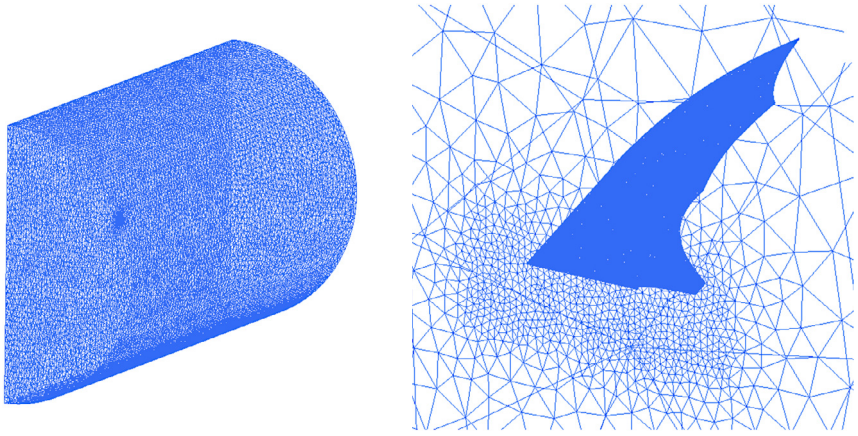

(a) Far field (b) Near wall

Fig. 4. Computational grid disposition.

$$f = \frac{m^{3/8} g^{1/2}}{b^{23/24} S^{1/3} \rho^{3/8}} = 4.71 \tag{4}$$

where m is the total mass, g is the gravitational acceleration, b is the length of the wing span, S is the total wing area and ρ is the density of the air.

According to Bullen and McKenzie [23], the flight speed of the large flying fox species is 3∼10 m/s, normally around 7 m/s at cruise. The cruise speed is therefore selected as 7 m/s in initial design. The Reynolds number of cruise is:

$$Re = \frac{V c_m}{\upsilon} = 114654 \tag{5}$$

where V is the cruise speed, c_m is the mean aerodynamic chord and υ is the kinematics viscosity which equals to the ratio of dynamic viscosity and density.

3. Aerodynamic analyses

3D aerodynamic analysis is an efficient way to assist the design of the flapping wing UAVs. The analysis is mostly based on CFD simulation [1,2,8,9,26–29] and wind tunnel experimental test [10,24,25]. In this paper, the aerodynamic analysis was processed based on CFD simulation. The wing platform was restricted to be rigid without passive deformation during flapping. Only aerodynamic lift was analyzed under different flight conditions to estimate the cruise ability. The thrust result obtained with the rigid model is unable to support the design process because of the ignorance of aeroelastic deformation. Thus the thrust result is not included for discussion in this paper. The software employed for simulation is ANSYS Fluent.

3.1. Numerical simulation

3.1.1. Simulation setup

Three dimensional CFD simulation was conducted to investigate the unsteady aerodynamics of the flapping wing UAV. A cylindrical far field was applied as the computational domain. The diameter of the inlet and outlet is 50c and the length of the field in flow direction is 100c. Boundary conditions of the far field and the wing are velocity inlet, outflow and no-slip wall. The symmetry boundary at x=0 is used in order to reduce the computational cost. Unstructured grid was adopted as shown in Fig. 4. The total number of the grid is 1.8 million. The minimum grid size on the wing surface is 0.005c in order to reflect the thickness of the wing.

Table 4
Specification of variables setting.

Variables	Value
Free stream velocity (m/s)	7
Flapping frequency (Hz)	3, 4, 5, 6, 7
Angle of attack (degree)	2, 4, 6, 8, 10

Unsteady pressure solver was employed in the simulation. Incompressible Reynolds-average Navier-Strokes (RANS) equations were solved by using finite volume method with SST k-ω turbulence model. In order to improve the accuracy of calculation, the SIMPLE scheme was employed for pressure-velocity coupling. The spatial discretization with second-order upwind scheme and the transient formulation with first-order implicit scheme were adopted. Further, the 0.001 second time step size was selected for unsteady simulation case of flapping motion. Time averaged aerodynamic force of one flapping cycle was used for analysis. The wing kinematics were defined in simulation cases followed by equation (1) and (2) as described in section 2.2. Dynamic mesh was employed for transient simulation of the flapping wing.

3.1.2. Variables setting

Specification of variables setting in CFD simulation is given in Table 4. The bat-inspired UAV is designed to cruise at the velocity of 7 m/s. In order to identify the aerodynamic performance of the UAV, five flapping frequencies from 3 Hz to 7 Hz and five angles of attack from 2 degrees to 10 degrees are selected for analysis. The CFD simulation is processed for five different flapping frequencies under each angle of attack.

3.2. Method validation

3.2.1. Solver validation

To validate the solver, aerodynamic analysis of a 3D flapping wing model from Zhang et al. [24] was investigated by comparing with wind tunnel data in published works [24,26]. The wing has a chord length 80 mm and semi-span length 135 mm. The computational grid is shown in Fig. 5. The validation model employed the unstructured grid, and the total grid number is 1.2 million. The condition of the test case including the angle of attack 7 degrees, free stream velocity 8 m/s and flapping frequency 7.8 Hz. Comparison result of CFD simulation and wind tunnel test in non-dimensional time is shown in Fig. 6. CFD result has a same periodicity with the wind tunnel data. The average lift of wind tunnel test is 27.49 g while the CFD result is 28.62 g. The lift re-

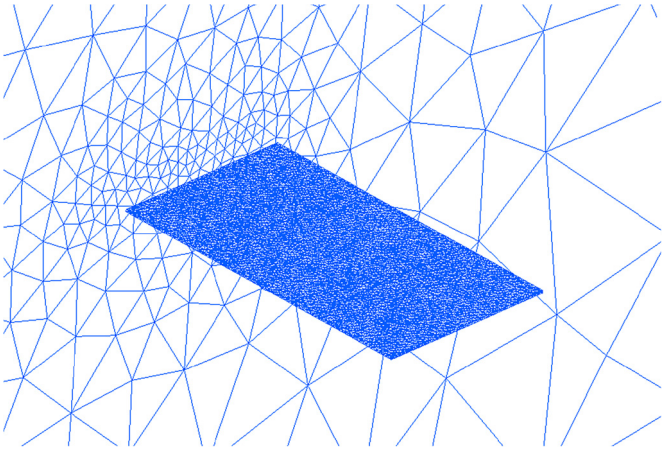

Fig. 5. Computational grid of the simulation method validation case.

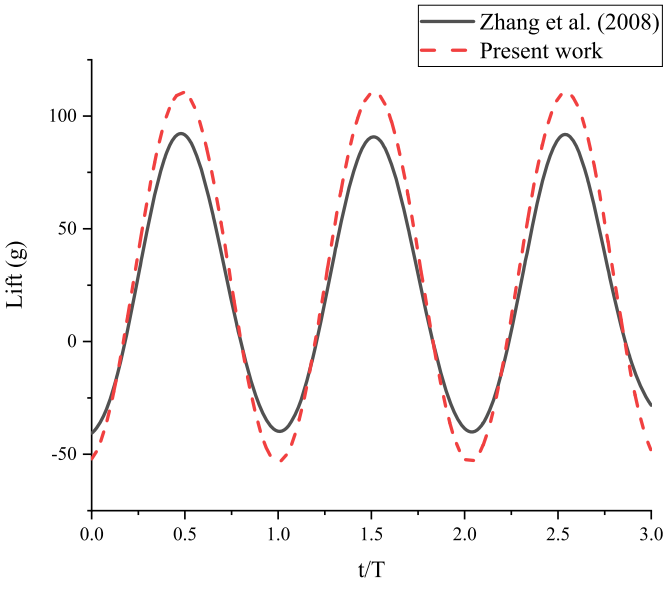

Fig. 6. Comparison of lift results of the solver validation case.

sult obtained from CFD simulation is only 4.1% more than the wind tunnel data. The difference is within 5% which shows a good agreement with the wind tunnel test.

3.2.2. Time step independence validation

Time step size validation was processed for the bat-inspired model before CFD analysis. Time step of 0.005 s, 0.001 s, and 0.0005 s are employed for simulation, respectively. Comparison result is provided in Fig. 7. As shown in Fig. 7, the lift resulted from time step size 0.001 s and 0.0005 s have no obvious difference. While the 0.005 s result has a 5.7% difference with the other two results, thus a time step size 0.001 s is employed for follow-up simulations.

3.3. Discussion of the numerical simulation results

3.3.1. Flow field discussion

Different with the fixed wing aircraft, the lift of flapping wing UAVs are generated based on unsteady aerodynamics [30]. The transient lift at each time step within one flapping cycle always has a large fluctuate which can be observed from Fig. 7. The lift curve in Fig. 7 experiences both positive and negative part during flapping, but the averaged lift within one cycle is positive, thus the UAV are able to fly. Spanwise pressure distribution also proves

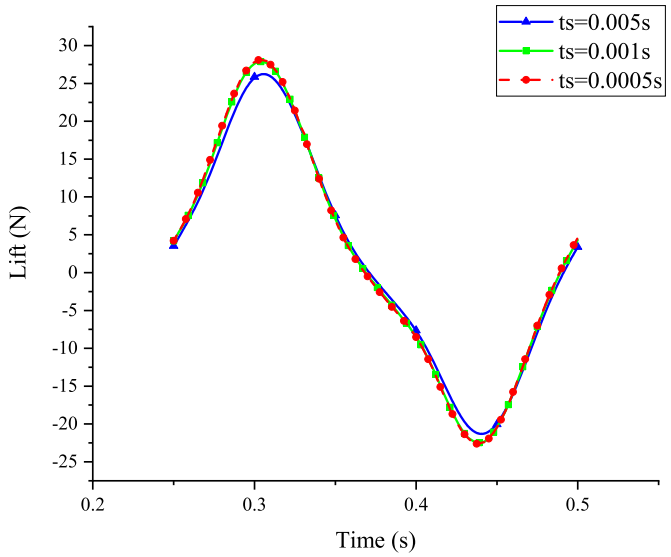

Fig. 7. Validation of time step size.

the result. Fig. 8 provides the spanwise pressure distribution at 2/8 T and 6/8 T where the maximum positive and negative force happened. From Fig. 8 it is able to observe that the pressure difference of the upper and lower surface during downstroke (2/8 T) is larger than the value during upstroke (6/8 T), thus the wing is able to generate a positive average lift with a full cycle of flapping motion.

Flapping wing UAVs also have a series of special lift enhancement mechanism [29–31], such as clip and fling, leading edge vortex (LEV) and wake capture. The lift generation process of the bat-inspired UAV is also benefited from the mechanism. Streamline along the flow direction at half inner wing span is proposed as shown in Fig. 9. It can be observed from the figure that a strong LEV appears on the upper surface of the wing during downstroke, and the vortex on the lower surface at the same flapping position during upstroke is not fully developed. The distribution of LEV resulted in a contribution to lift generation.

3.3.2. The influence of angle of attack on average lift performance

The results of average lift and lift coefficient variation with respect to angle of attack at five different flapping frequencies are shown in Fig. 10. It can be seen that the average lift increases with the increasing of UAV angle of attack. The aerodynamic lift increases almost linearly from 2 to 10 degrees. The lift slopes for different flapping frequency are about the same. As can be obtained from Fig. 10, the UAV is able to achieve cruising at the angle of attack and flapping frequency conditions 2.4 degrees, 4 Hz or 5.5 degrees, 3 Hz.

3.3.3. The influence of flapping frequency on average lift performance

The results of average lift and lift coefficient variation with respect to the flapping frequency in five angle of attack conditions are shown in Fig. 11. The average lift generated by wing flapping is increasing with the flapping frequency increased from 3 Hz to 7 Hz. The slope of the lift appears to be decreasing at the flapping frequency lower than 5 Hz, and then becomes steady at higher frequencies, resulted a linearly increasing of the aerodynamic lift. It can be observed from Fig. 11 that the UAV is able to achieve the cruise condition at the angle of attack and flapping frequency condition 4 degrees, 3.5 Hz or 2 degrees, 4.5 Hz. The four possible conditions for cruise are summarized in Table 5.

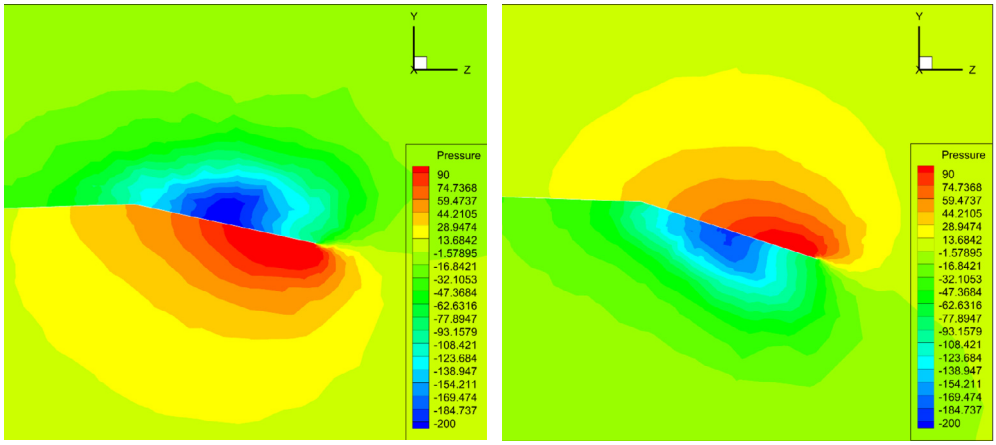

(a) t = 2/8 T (b) t = 6/8 T

Fig. 8. Pressure distribution along the spanwise at 0.25 chord position. (For interpretation of the colors in the figures, the reader is referred to the web version of this article.)

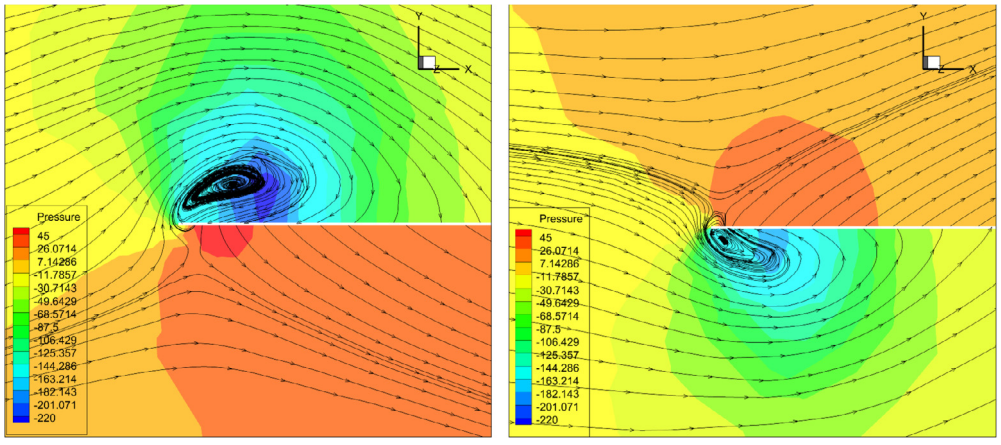

(a) t = 2/8 T (b) t = 6/8 T

Fig. 9. Pressure distribution with streamline along flow direction (0.5 inner wing span). (For interpretation of the colors in the figures, the reader is referred to the web version of this article.)

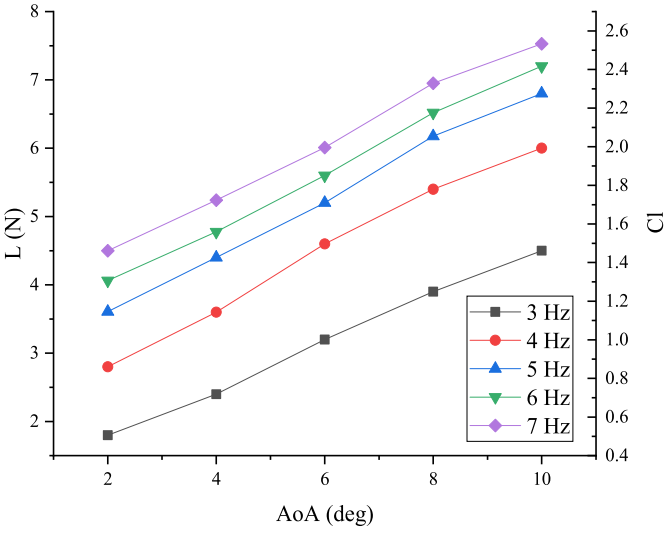

Fig. 10. Average lift and lift coefficient results with respect to angle of attack.

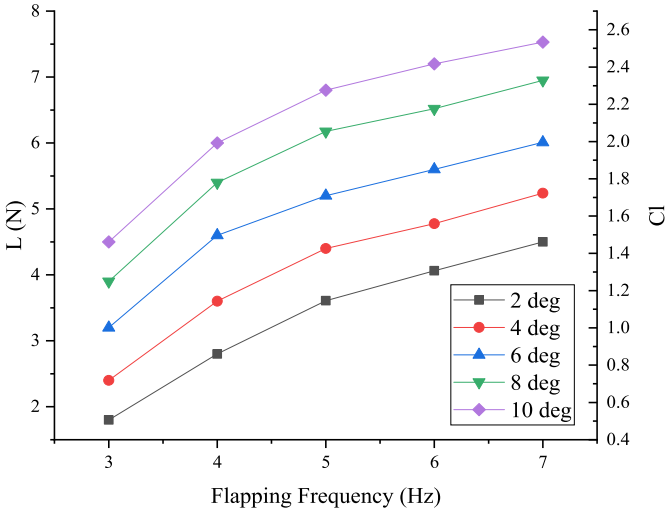

Fig. 11. Average lift and lift coefficient results with respect to flapping frequency.

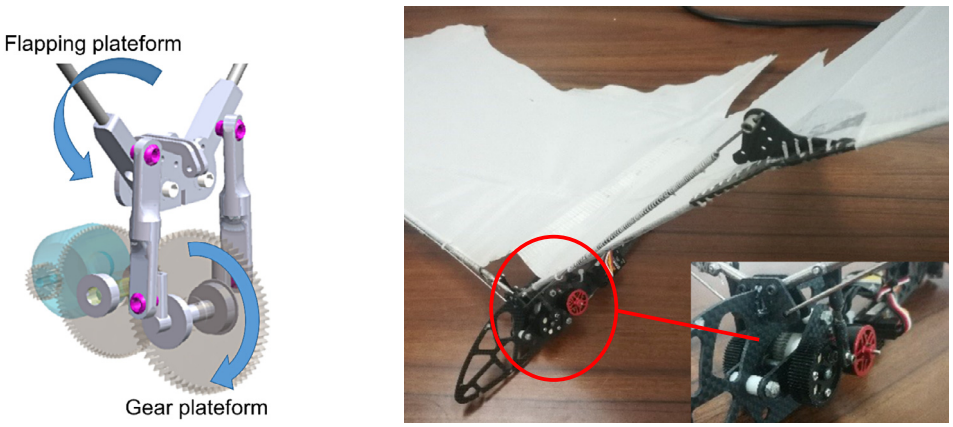

(a) Speed reduction gearbox (b) Assembled flapping mechanism

Fig. 12. Flapping mechanism.

Table 5
Specification of possible cruise conditions.

Conditions	Angle of attack (deg)	Flapping frequency (Hz)
Condition 1	2	4.5
Condition 2	2.4	4
Condition 3	4	3.5
Condition 4	5.5	3

4. Manufacture and test flight

4.1. Flapping mechanism

The flapping mechanism employs a 2-DOFs revolute-spherical-spherical-revolute (RSSR) mechanism in order to reflect the larger displacement attitude of the wing tip during downstroke. The geometry of the RSSR mechanism is shown in Fig. 12 (a), the role of the mechanism is to transfer the motion from the gear platform into the flapping platform. The maximum rotation frequency of the selected DC motor is 314.5 Hz at the applied voltage 11.1 V with maximum throttle level. Assuming that the motor is rotating at 50% of the maximum throttle level during cruise, with the designed flapping frequency 3.5 Hz, the transmission ratio is calculated to be 44.92. Detailed gear parameters are designed to achieve the speed reduction. The gear is manufactured through 3D print with engineering plastic material. The CAD model of the gearbox and the assembled flapping mechanism onboard are shown in Fig. 12.

4.2. Manufactured prototype

The prototype consists of the frame, onboard devices and battery. In terms of the frame of the UAV, carbon fiber composite material is used for all structural components including fuselage and skeleton of wing and control surface. Polyester fiber material is selected for skin membrane. The onboard devices of the bat-inspired UAV including one brushless DC motor, one electronic speed controller, one flight controller, a signal receiver and two steering actuators for elevon control. Manufactured prototype with onboard devices is shown in Fig. 13. With the onboard devices all equipped, the total mass of the bat-inspired UAV is 289 g. It is proved by CFD simulation that the lift generated by the UAV with the design condition is able to support the cruise.

4.3. Test flight

Test flight has been processed with the manufactured bat-inspired UAV model. Hand launch was employed for take-off. The

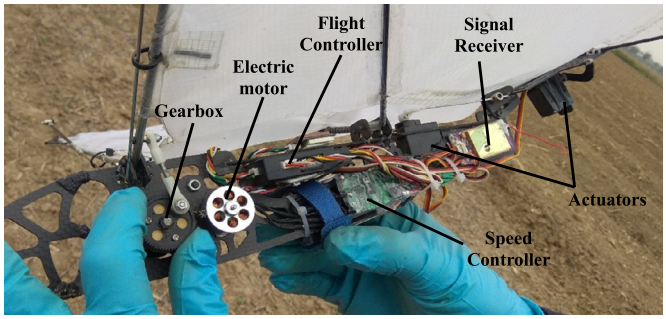

Fig. 13. Onboard devices.

UAV carried an onboard FDR in order to record the position and attitude data during flying. The pictures of the UAV model and attitude during flight are shown in Fig. 14.

Flight trajectory and performance data were obtained from the onboard FDR. The data of the circular cruise trajectory is shown in Fig. 15. The x, y and z coordinate present east longitude position, north latitude position, and height position, respectively. It can be seen that the UAV launched from the launch-and-recovery position, which has been circled out in Fig. 15, and then climbed to the cruise altitude. The UAV then continued a cruise based on a circular route, and then declined and landed to the same position where launched. Fig. 16 presented the flight speed, pitch angle, roll angle and flight direction angle data obtained from the FDR. It is able to observe from Fig. 16 (d) that the UAV can keep a steady turn angle to achieve the circular route. The large fluctuation of the data near 150 second is because the inboard data recorder for direction angle has no negative value. The yaw attitude is fluctuating around 0 degree thus resulted the data variation around 0 degrees and 360 degrees. The periodicity from the pitching angle can reflect the flapping frequency during flight as shown in Fig. 16 (e). Average values were obtained based on linear polynomial fitting. Result shows that the average cruise speed is 6.8 m/s while the flapping frequency is about 3.7 Hz. The time averaged pitching angle is 4.1 degrees. Test flight data shown a good agreement with the CFD result of Condition 3 in Table 4. Other possible conditions were also employed during test flight but were unable to support a stable cruise. The reason is probably because the thrust generated by the other three conditions is unable to balance the drag during flight.

An interesting phenomenon is that the velocity curve in Fig. 16 (a) has a periodical variation during the flight. The period is about 40 seconds which seems not to be the flapping frequency. A rea-

(a) Cruising

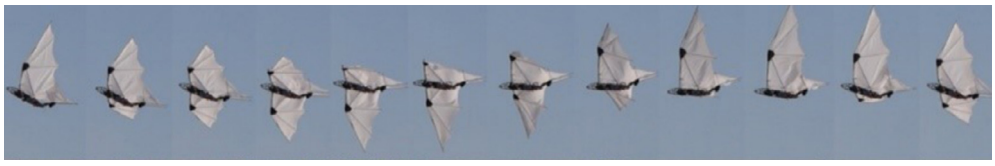

(b) Flapping attitude through one flapping cycle

Fig. 14. Test flight.

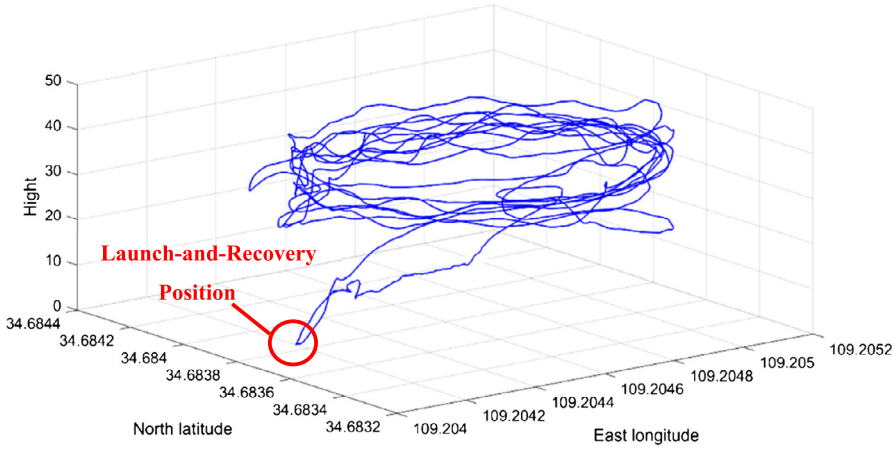

Fig. 15. Flight trajectory.

soning is made at present that the phenomenon is due to a steady direction of wind. Because the period is well matched with the number of circles during cruise as shown in Fig. 15, and the result will be a sine wave as shown in Fig. 16 (a) if the wind speed is steadily 3 m/s. It can also get proved from Fig. 16 (d) that the flight direction angle keeps a same periodicity with the long period speed variation. However, there are still other possibilities such as a long periodic oscillation which always appears in flight dynamics of the tailless model, which needed further analysis in the future.

The test proved that the designed bat-inspired flapping wing UAV is able to propose a stable flight. The UAV is able to achieve a steady circular cruise. The endurance of the UAV in the outdoor environment with the onboard battery can reach more than 5 minutes with the designed cruise condition.

5. Conclusions

This paper proposed a design and test process of a bat-inspired tailless flapping wing UAV. The geometry parameter is designed based on bionic similarity, and the aerodynamic characteristics are calculated based on CFD simulations. Outdoor test flight is processed with the manufactured prototype. Conclusions are as follows,

1. The UAV is able to process an outdoor cruise, which proves that the tailless configuration is suit for the design of flapping wing UAV. The tested UAV equipped payload including flight controller and FDR which are able to work well during flight. The successful cruise test provides more possibility for future design of flapping UAV.
2. Numerical simulation is able to support the analysis at the initial design stage. With the same cruise speed, the result of design variables obtained from CFD simulation matched well with the test flight result. The flapping frequency and the angle of attack obtained based on CFD simulation are only 5.4% and 2.5% difference compared with the test flight results.
3. Based on the result of CFD simulation, the bat-inspired UAV has the prospect to support a higher take-off weight with a different selection of frequency and angle of attack condition.

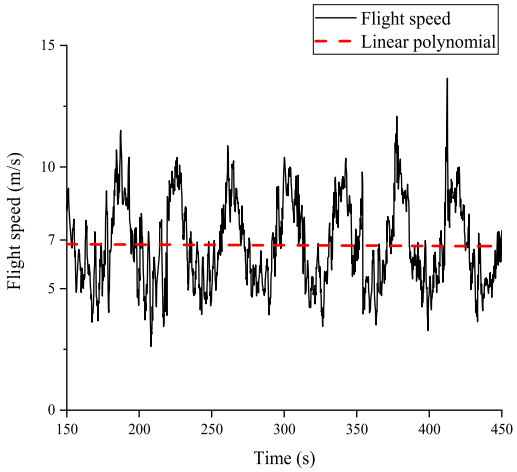

(a) Flight speed with respect to time

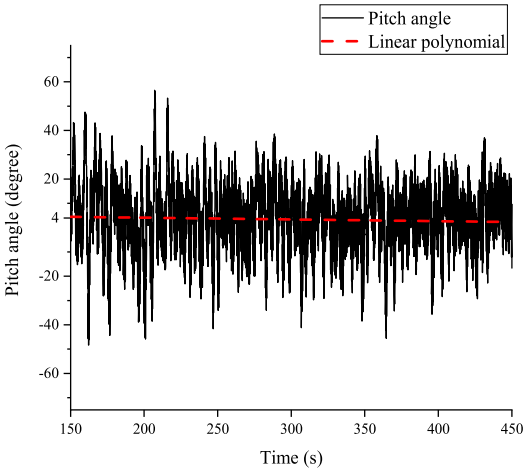

(b) Pitch angle with respect to time

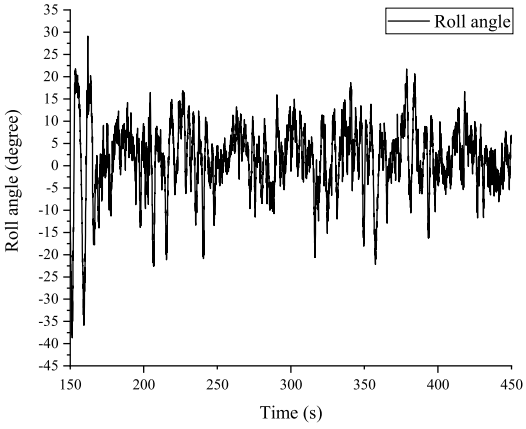

(c) Roll angle with respect to time

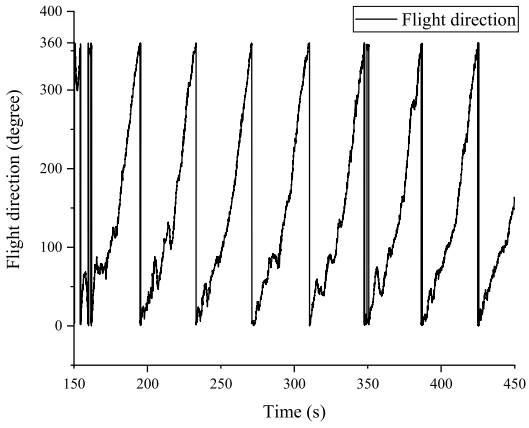

(d) Flight direction angle with respect to time

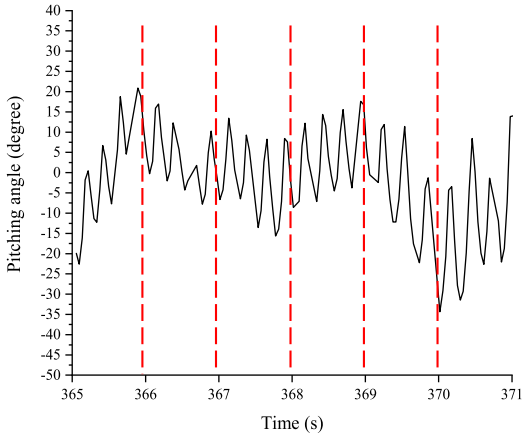

(e) Periodicity of pitching angle

Fig. 16. Flight data.

This gives the UAV a practicable large payload capacity, which is useful in future applications and researches.

Declaration of competing interest

The authors declare that they have no known competing financial interests or personal relationships that could have appeared to influence the work reported in this paper.

Acknowledgements

This study was supported by the National Natural Science Foundation of China (No. 11972059 and No. 11902018).

References

[1] S. Chen, H. Li, S. Guo, M. Tong, B. Ji, Unsteady aerodynamic model of flexible flapping wing, Aerosp. Sci. Technol. 80 (2018) 354–367.

[2] Y. Bayiz, S.-J. Hsu, A. Aguiles, Y. Alexander, B. Chen, Experimental learning of a lift-maximizing central pattern generator for a flapping robotic wing, in: 2019 International Conference on Robotics and Automation (ICRA), Montreal, Canada, May 20–24, 2019.
[3] C. Galiński, R. Żbikowski, Insect-like flapping wing mechanism based on a double spherical Scotch yoke, J. R. Soc. Interface 2 (2005) 223–235.
[4] R. Żbikowski, C. Galiński, C.B. Pedersen, Four-bar linkage mechanism for insect like flapping wings in hover: concept and an outline of its realization, J. Mech. Des. 127 (2005) 817–824.
[5] H. Phan, Q. Nguyen, Q. Truong, T. Truong, H. Park, N. Goo, D. Byun, M. Kim, Stable vertical takeoff of an insect-mimicking flapping-wing system without guide implementing inherent pitching stability, J. Bionics Eng. 9 (2012) 391–401.
[6] M. Karásek, F.T. Muijres, C. de Wagter, B. Remes, G. de Croon, A tailless aerial robotic flapper reveals that flies use torque coupling in rapid banked turns, Science 361 (2018) 1089–1094.
[7] C.J. Pennycuick, Modelling the Flying Bird, Academic Press, Elsevier, Netherlands, 2008.
[8] C. Gong, J. Han, Z. Yuan, Z. Fang, G. Chen, Numerical investigation of the effects of different parameters on the thrust performance of three dimensional flapping wings, Aerosp. Sci. Technol. 84 (2019) 431–445.
[9] D. Xue, B. Song, W. Song, W. Yang, W. Xu, T. W, Computational simulation and free flight validation of body vibration of flapping wing MAV in forward flight, Aerosp. Sci. Technol. 95 (2019) 105491.
[10] K. Mazaheri, A. Ebrahimi, Experimental investigation on aerodynamic performance of a flapping wing vehicle in forward flight, J. Fluids Struct. 27 (2011) 586–595.
[11] W. Yang, L. Wang, B. Song, Dove: a biomimetic flapping-wing micro air vehicle, Int. J. Micro Air Veh. 10 (2017) 70–84.
[12] B.-J. Tsai, Y.-C. Fu, Design and aerodynamic analysis of a flapping-wing micro aerial vehicle, Aerosp. Sci. Technol. 13 (2009) 383–392.
[13] W.-B. Gan, Research on aerodynamic numerical simulation and design of near space low-Reynolds-number unmanned aerial vehicles, Ph.D. Dissertation, Northwestern Polytechnical University, Xi'an, 2014.
[14] S. Wang, X. Zhang, G. He, T. Liu, Numerical simulation of unsteady flows over a slow-flying bat, Theor. Appl. Mech. Lett. 5 (2015) 5–8.
[15] J.W. Bahlman, S.M. Swartz, K.S. Breuer, Design and characterization of a multi-articulated robotic bat wing, Bioinspir. Biomim. 8 (2013) 016009.
[16] F.T. Muijres, P. Henningsson, M. Stuiver, A. Hedenstrom, Aerodynamic flight performance in flap-gliding birds and bats, J. Theor. Biol. 306 (2012) 120–128.
[17] Y. Yu, Z. Guan, Learning from bat: aerodynamics of actively morphing wing, Theor. Appl. Mech. Lett. 5 (2015) 13–15.
[18] M.F. Bin Abas, A.S. Bin Mohd Rafie, H. Bin Yusoff, K.A. Bin Ahmad, Flapping wing micro-aerial-vehicle: kinematics, membranes, and flapping mechanisms of ornithopter and insect flight, Chin. J. Aeronaut. 29 (2016) 1159–1177.
[19] A. Ramezani, S. Chung, S. Hutchinson, A biomimetic robotic platform to study flight specializations of bats, Sci. Robot. 2 (2017) eaal2505.
[20] J.A. Cheney, D. Ton, N. Konow, D.K. Riskin, K.S. Breuer, S.M. Swartz, Hindlimb motion during steady flight of the lesser dog-faced fruit bat, Cynopterus brachyotis, PLoS ONE 9 (2014) e98093.
[21] M. Wolf, L.C. Johansson, R. von Busse, Y. Winter, A. Hedenstrom, Kinematics of flight and the relationship to the vortex wake of a Pallas' long tongued bat (Glossophaga soricina), J. Exp. Biol. 213 (2010) 2142–2153.
[22] D.K. Riskin, J. Iriarte, K.M. Middleton, K.S. Breuer, S.M. Swartz, The effect of body size on the wing movements of pteropodid bats, with insights into thrust and lift production, J. Exp. Biol. 213 (2010) 4110–4122.
[23] R.D. Bullen, N.L. McKenzie, Scaling bat wingbeat frequency and amplitude, J. Exp. Biol. 205 (2002) 2615–2626.
[24] Y. Zhang, B. Song, C. Yuan, G. Ji, Lift characteristic of the flapping wing micro air vehicle, Acta Aerodyn. Sin. 26 (2008) 519–522.
[25] S. Deng, J. Wang, H. Liu, Experimental study of a bio-inspired flapping wing MAV by means of force and PIV measurements, Aerosp. Sci. Technol. 94 (2019) 105382.
[26] K. Liu, D. Li, J. Xiang, Reduced-order modeling of unsteady aerodynamics of a flapping wing based on the Volterra theory, Results Phys. 7 (2017) 2451–2457.
[27] A.H. Ahmed, E.S. Ahmed, E.T. Haithem, R.H. Muhammad, Optimal transition of flapping wing micro-air vehicles from hovering to forward flight, Aerosp. Sci. Technol. 90 (2019) 246–263.
[28] W. Tay, B. Oudheusden, H. Bijl, Numerical simulation of a flapping four-wing micro-aerial vehicle, J. Fluids Struct. 55 (2015) 237–261.
[29] D. Bie, S. Zuo, H. Li, H. Shao, D. Li, Aerodynamic analysis of a gull-inspired flapping wing glider, in: 4th International Conference on Aeronautical Materials and Aerospace Engineering (AMAE 2020), Chengdu, China, 14–17 May, 2020.
[30] W. Shyy, H. Aono, S.K. Chimakurthi, P. Trizila, C.K. Kang, C. Cesnik, H. Liu, Recent progress in flapping wing aerodynamics and aeroelasticity, Prog. Aerosp. Sci. 46 (2010) 284–327.
[31] D. Chin, D. Lentink, Flapping wing aerodynamics: from insects to vertebrates, J. Exp. Biol. 219 (2016) 920–932.